Available online at www.sciencedirect.com
SCIENCE DIRECT®
Comput. Methods Appl. Mech. Engrg. 194 (2005) 1225–1248
Computer methods in applied mechanics and engineering
www.elsevier.com/locate/cma

On the interaction between dynamic model dissipation and numerical dissipation due to streamline upwind/Petrov–Galerkin stabilization

Andrés E. Tejada-Martínez *,[1], Kenneth E. Jansen

Scientific Computation Research Center and Mechanical, Aerospace and Nuclear Engineering, Rensselaer Polytechnic Institute, Troy, NY, USA

Received 2 June 2003; received in revised form 20 January 2004; accepted 8 June 2004

Abstract

Here we investigate the roles of physical and numerical subgrid-scale modeling. The subgrid-scales are represented by a physical large-eddy simulation model, namely the popular dynamic Smagorinsky model (or simply dynamic model), as well as by a numerical model in the form of the well-known streamline upwind/Petrov–Galerkin stabilization for finite element discretizations of advection–diffusion systems. The latter is not a physical model, as its purpose is to provide sufficient algorithmic dissipation for a stable, consistent, and convergent numerical method. We study the interaction between the physical and numerical models by analyzing energy dissipation associated to the two. Based on this study, a modification to the dynamic model is proposed as a way to discount the numerical method's algorithmic dissipation from the total subgrid-scale dissipation. The modified dynamic model is shown to be successful in simulations of turbulent channel flow.

1. Introduction

The classical Galerkin method for the incompressible Navier–Stokes equations is well-known to be unstable in the advective dominated limit, as discussed in [3]. A second instability can occur for certain interpolation combinations of the velocity and pressure which violate the so-called Babuška–Brezzi

* Corresponding author.
[1] Present address: Center for Coastal Physical Oceanography, Old Dominion University, Crittenton Hall, 768 West 52nd Street, Norfolk, VA 23529, USA.

0045-7825/$ - see front matter
doi:10.1016/j.cma.2004.06.037

condition. In Refs. [3,9] among others, streamline upwind/Petrov–Galerkin (SUPG) stabilization has been shown to remedy these instabilities through the addition of numerical diffusion along streamlines. In [8] and more recently in [4], the origins of such stabilized methods are brought to light, being interpreted as subgrid-scale (SGS) numerical models which account for the effect of small scales, unresolvable by the discretization, on the resolvable large scales. More precisely, as discussed in [1], stabilization can be thought of as the enrichment of the finite dimensional space underlying the discretization (which can only represent scales larger than a certain size) through the addition of a higher order function, the so called residual-free bubble.

In large-eddy simulation (LES) of turbulent flows, a spatial filter is applied to the Navier–Stokes equations with the purpose of filtering out small scales and thereby allowing coarser discretizations to solve for the large (resolved) scales governed by the filtered equations. The filtering operation splits a field into filtered and residual components, and furthermore, in the case of the filtered Navier–Stokes equations, this operation generates an unknown residual stress tensor reflecting the effect of the residual scales on the filtered scales. In practice, the discretization (in our case the SUPG method) assumes the role of the spatial filter, thus the residual component of the original field can be regarded as the subgrid component and the residual stress can be regarded as the subgrid stress. The latter has traditionally been referred to as the SGS stress. Given that the SGS stress is unknown, it must be represented through an SGS model. To that extent, we will use the dynamic coefficient Smagorinsky model (dynamic model), developed in [5] and [15].

It is clear from the previous interpretations that although motivated by different needs, subgrid-scale models in LES and stabilization operators in otherwise unstable classical Galerkin discretizations share similar purposes. Both aim at representing the effect of unresolved small scales on resolved large scales by introducing proper dissipative mechanisms. The phrase ''proper dissipative mechanisms'' deserves special attention. In the case of stabilized methods, artificial energy dissipation is introduced for the purpose of achieving a stable, consistent and convergent discretization, thereby making the stabilization operator strictly grid dependent. In the case of LES, dissipation is introduced not to provide stability but to model the cascading transfer of energy that occurs between large and small scales in a turbulent flow. As viewed in [21] and later noted in [20], although the physical SGS model can be effected by numerical issues, in principle it should be independent of the numerical method. The effectiveness of the physical model should be based solely on how well it describes the residual stress. For example, the dynamic mixed model developed in [29] and references within is well known to be superior to the classic dynamic model because the modeled residual stress is better aligned with the true residual stress which can be measured through direct numerical simulation.

There are differing viewpoints on the role of numerical dissipation in LES. The simplest is that grid spacing should be chosen sufficiently small so that numerical dissipation is negligible compared to physical dissipation. In the variational multi-scale approach to LES in [10], the roles of numerical and physical dissipation are hypothesized. In the previous work, the substitution of numerical dissipation (applied to the smallest resolvable scales) by physical dissipation is considered. The remark is made that physical dissipation could be sufficient to stabilize the smaller resolvable scales, but artificial dissipation is still required to stabilize the larger resolvable scales. The authors in [10] conjecture that ideally, artificial, numerical dissipation should not greatly degrade or interfere with the behavior of the physical model. However, it is noted that tuning of parameters associated to numerical dissipation might be required to produce the desired energy transfer between the larger and smaller resolved scales. In principle, this should not be the case.

The opposite viewpoint, advocated by Boris et al. [2], is that no explicit physical SGS model is required if an appropriate method providing sufficient, proper numerical dissipation is used. Boris et al. refer to this approach as monotone integrated large-eddy simulation (MILES). In addition to the works cited by Boris et al., other works using the MILES approach are [24,14,19]. The main advantage of the MILES approach is that the effort required to develop physical SGS models is eliminated. However, physical modeling and the numerics are inseparably intertwined. For a given LES, results depend on the numerical method and on the grid used, as it is not possible to refine the grid to obtain grid-independent solutions. Refining the grid in

search of grid-independence would lead to a DNS, no longer LES. Furthermore, not all numerical methods are suited for the MILES approach. The SUPG method used here is not, as is shown in [26].

There have been some researchers that have tried to understand the behavior of the physical SGS model in the presence of numerical dissipation. In Ref. [18], the effect of artificial dissipation on the physical SGS model is investigated by tracking the dynamic model's eddy viscosity when dissipative and non-dissipative discretizations are used. The influence of the model increases when the non-dissipative solver is used instead of the dissipative solver, suggesting that the model is robust enough to adjust for numerical diffusion.

Given the unavoidable coupling between the physics and the numerics, in this work we explore the interaction between physical and numerical subgrid-scale models by tracking the physical model dissipation, as well as our own definition of numerical dissipation due to SUPG stabilization. It is seen that for low Reynolds number channel flow simulations on relatively coarse grids, which lead to numerical dissipation on the same order but still smaller than physical model dissipation, numerical dissipation does play a role. It will be shown that the model does not adjust well enough in the presence of changing numerical dissipation, contrary to previous belief. To this end, we will introduce a correction to the model, which will serve essentially as a coupling between the model and stabilization at the energy dissipation level. This coupling will lead to a model independent of the amount of numerical subgrid-scale energy dissipation present in the simulations performed here, as it should be in principle. To date, this is the first attempt at physical modeling of the subgrid-scale stress taking into account the presence of numerical dissipation.

2. Mathematical preliminaries

2.1. The filtered incompressible Navier–Stokes equations

In LES, the large-scale quantities are resolved and the small-scale quantities are modeled. The large-scale quantities are defined by a low-pass filtering operation given as

$$\bar{f}(\boldsymbol{x}) = \int G_{\overline{\Delta}}(\boldsymbol{x},\boldsymbol{y}) f(\boldsymbol{y})\,\mathrm{d}\boldsymbol{y}, \tag{1}$$

where $G_{\overline{\Delta}}$ is the filter kernel and the integration is extended over the entire domain. Filters of small support with size on the order of $\overline{\Delta}$ are used, thus, the previous integral is essentially a local weighted average of the original function about the point $\boldsymbol{y} = \boldsymbol{x}$. The original function $f(\boldsymbol{x})$ is decomposed into a resolved or filtered component ($\bar{f}(\boldsymbol{x})$) and a lost residual component characterized by scales on the order of the filter width $\overline{\Delta}$.

If the kernel $G_{\overline{\Delta}}$ is homogeneous, the filtering operation commutes with differentiation. Hence, application of a homogeneous filter to the Navier–Stokes equations, renders the continuity and momentum equations (the latter in conservation form) as

$$\begin{aligned} &\bar{u}_{i,i} = 0 \\ &\bar{u}_{i,t} + (\bar{u}_i \bar{u}_j)_{,j} = -\overline{P}_{,i} + (\overline{\tau^{\mathrm{v}}}_{ij} - \tau_{ij})_{,j}, \end{aligned} \tag{2}$$

respectively, where $\bar{u}_i$ is the ith component of the filtered velocity, $\overline{P}$ is the filtered pressure divided by constant density ρ, and $\overline{\tau^{\mathrm{v}}_{ij}}$ is the filtered viscous stress tensor given by

$$\overline{\tau^{\mathrm{v}}_{ij}} = \nu(\bar{u}_{i,j} + \bar{u}_{j,i}). \tag{3}$$

Here $\nu = \mu/\rho$ is the kinematic viscosity, where μ is the molecular viscosity. The summation convention (implying a sum on repeated indices) is used in the previous expressions and will be used throughout this work.

In addition to the filtered viscous stress, the filtered equations also have a residual or SGS stress defined as

$$\tau_{ij} = \overline{u_i u_j} - \bar{u}_i \bar{u}_j, \tag{4}$$

generated by the filtering operation and reflecting the effect of the filtered-out residual scales on the resolved scales. The trace of the residual stress is absorbed into the filtered pressure and the deviatoric portion is modeled.

Given a model for the SGS stress, the equations in (2) are solved for the resolved velocity and pressure. In practice, the filtering operation applied to the original (unfiltered) Navier–Stokes equations is not applied before hand. It is defined by the discretization which serves as a filter because it can not resolve all of the scales present in a turbulent flow, unless the grid is refined enough. This is precisely why the filter with kernel $G_{\overline{\Delta}}$, used to obtain the filtered equations, is often referred to as the grid filter.

2.2. The SGS dynamic model

In this work we focus on the dynamic formulation of the Smagorinsky eddy viscosity (ν_T) model [23]. The Smagorinsky model expresses the deviatoric part of the SGS stress as

$$\tau_{ij}^d = \tau_{ij} - \frac{1}{3}\tau_{kk}\delta_{ij} = -2\underbrace{(C_s\overline{\Delta})^2 \mid \bar{S} \mid}_{\text{eddy viscosity}} \overline{S}_{ij}, \tag{5}$$

where $\overline{\Delta}$ is the width of the grid filter, C_s the Smagorinsky constant, $\overline{S}_{ij} = (\bar{u}_{i,j} + \bar{u}_{j,i})/2$ the filtered strain-rate tensor, and $\mid \overline{S} \mid = (2\overline{S}_{ij}\overline{S}_{ij})^{1/2}$ is its norm. In the formulation of [5] and [15], the model coefficient is computed dynamically as

$$(C_s\overline{\Delta})^2 = \frac{1}{2}\frac{\langle L_{ij}M_{ij}\rangle}{\langle M_{kl}M_{kl}\rangle}, \tag{6}$$

where

$$L_{ij} = \widehat{\bar{u}_i\bar{u}_j} - \widehat{\bar{u}}_i\widehat{\bar{u}}_j, \tag{7}$$

and

$$M_{ij} = \widehat{\mid \overline{S} \mid \overline{S}}_{ij} - \alpha \mid \widehat{\overline{S}} \mid \widehat{\overline{S}}_{ij}. \tag{8}$$

Application of a homogeneous low-pass test filter is denoted with an over-hat, $\widehat{\cdot}$. The angle brackets in (6) denote averaging in spatial homogeneous directions as means of preventing instabilities due to potential negative values of the model coefficient. Finally, α is a parameter denoting the filter width ratio, related to the width of the test and grid filters. In our simulations, we compute this ratio based on the standard deviation of the test filters used as a way to define the filter width. We take the filter width ratio as simply the test filter width divided by the mesh size. Extensive discussions on the filter width ratio and how to compute test filter widths are given in [27] and [16].

2.3. Resolved kinetic energy

To study the effect of the physical SGS dynamic model and its interaction with numerical dissipation, dissipation due to the physical SGS stress is of importance. To that extent, we consider the transport equation for the resolved energy $k = \bar{u}_i\bar{u}_i/2$, found by dotting the filtered momentum equation in (2) with the velocity vector:

$$\dot{k} + (\bar{u}_j k)_{,j} = (-\bar{u}_j \overline{P} + \bar{u}_i \overline{\tau^v_{ij}} - \bar{u}_i \tau^d_{ij})_{,j} - \overline{\tau^v_{ij}} \overline{S}_{ij} + \tau^d_{ij} \overline{S}_{ij}, \tag{9}$$

where $\overline{P}$ is the filtered pressure divided by density plus a term containing the trace of the SGS stress. The divergence terms in the right hand side of (9) serve to re-distribute the resolved kinetic energy. The other terms in the right hand side of (9) may represent a loss or gain of resolved kinetic energy. For example, if the term $\tau^d_{ij}\overline{S}_{ij}$ (the last term in (9)) is negative, the subgrid-scales remove energy from the resolved ones, often referred to as forward scatter or dissipation. On the other hand, if this term is positive, the subgrid-scales give energy to the resolved ones, often referred to as backscatter. In the dynamic model considered here, the majority of instances the eddy viscosity is positive due to averaging of the numerator and denominator in the model coefficient in (6), resulting in

$$\tau^d_{ij}\overline{S}_{ij} = -2\nu_T \overline{S}_{ij}\overline{S}_{ij} < 0, \tag{10}$$

thus only forward scatter or dissipation. In (10) we have used the fact that the trace-free residual stress tensor is expressed through the Smagorinsky model as $\tau^d_{ij} = -2\nu_T \overline{S}_{ij}$. The eddy viscosity ν_T is obtained dynamically as $\nu_T = (C_s\overline{\Delta})^2 \mid \overline{S} \mid$. Herein we refer to $-2\nu_T \overline{S}_{ij}\overline{S}_{ij}$ as the physical SGS energy dissipation, traditionally referred to as simply SGS dissipation. This is a misnomer given that in some instances numerical dissipation is also a type of SGS dissipation, such as is the case with the SUPG method.

2.4. Weak form—finite element discretization with the SUPG method

Next, we proceed with the stabilized finite element discretization of the weak form of the modeled, filtered Navier–Stokes equations (the filtered continuity (first) equation in (2) and the filtered momentum equation in (2)). First, we introduce the discrete weight and solution function spaces that are used. Let $\overline{\Omega} \subset \boldsymbol{R}^N$ represent the closure of the physical spatial domain, $\Omega \cup \Gamma$, in N dimensions; only $N = 3$ is considered. The boundary, Γ, is decomposed into portions with natural boundary conditions, Γ_h, and essential boundary conditions, Γ_g, i.e., $\Gamma = \Gamma_g \cup \Gamma_h$. In addition, $H^1(\Omega)$ represents the usual Sobolev space of functions with square-integrable values and derivatives on Ω (see Hughes [11]).

Subsequently Ω is discretized into n_{el} finite elements, $\overline{\Omega}_e$, where $\overline{\Omega}_e$ denotes the closure of finite element e. With this, we can define the discrete trial solution and weight spaces for the semi-discrete formulation as

$$\begin{aligned}
\mathscr{S}^p_h &= \{\boldsymbol{v} \mid \boldsymbol{v}(\cdot,t) \in H^1(\Omega)^N, t \in [0,T], \boldsymbol{v}|_{x\in\overline{\Omega}_e} \in P_p(\overline{\Omega}_e)^N, \boldsymbol{v}(\cdot,t) = \boldsymbol{g} \text{ on } \Gamma_g\},\\
\mathscr{W}^p_h &= \{\boldsymbol{w} \mid \boldsymbol{w}(\cdot,t) \in H^1(\Omega)^N, t \in [0,T], \boldsymbol{w}|_{x\in\overline{\Omega}_e} \in P_p(\overline{\Omega}_e)^N, \boldsymbol{w}(\cdot,t) = \boldsymbol{0} \text{ on } \Gamma_g\},\\
\mathscr{P}^p_h &= \{p \mid p(\cdot,t) \in H^1(\Omega), t \in [0,T], p|_{x\in\overline{\Omega}_e} \in P_p(\overline{\Omega}_e)\},
\end{aligned} \tag{11}$$

where $P_p(\overline{\Omega}_e)$ is the piecewise polynomial space, complete to order p, defined on $\overline{\Omega}_e$. In this work we will perform simulations with piecewise tri-linear basis functions, restricting to $p = 1$. Let us emphasize that the local approximation space, $P_p(\overline{\Omega}_e)$, is the same for both the velocity and pressure variables. This is possible due to the stabilized nature of the formulation to be introduced below. These spaces represent discrete subspaces of the spaces in which the weak form is defined.

The stabilized formulation used in the present work is an alternative to that described in [25] and furthermore used in [28] with great success. The authors in the previous two references work with the advective form of the incompressible equations. Here we will work with the conservative form of these equations for reasons to become apparent in the next sub-section.

The current weak formulation of the conservative form of the incompressible, modeled, filtered equations proceeds as follows. Given the spaces previously defined, we first present the semi-discrete Galerkin finite element formulation applied to the weak form of the modeled, filtered equations as:

Find $\boldsymbol{u} \in \mathscr{S}_h^p$ and $P \in \mathscr{P}_h^p$ such that

$$B_G(w_i, q; u_i, P) = 0$$

$$B_G(w_i, q; u_i, P) = \int_\Omega \{w_i \dot{u}_i + w_{i,j}(-u_i u_j - P\delta_{ij} + \tau^*_{ij}) - q_{,i} u_i\}\,\mathrm{d}x + \int_{\Gamma_h} \{w_i(u_i u_n + P\delta_{in} - \tau^*_{in}) + q u_n\}\,\mathrm{d}s \tag{12}$$

for all $\boldsymbol{w} \in \mathscr{W}_h^p$ and $q \in \mathscr{P}_h^p$. Note that the stress τ^*_{ij} is given as the viscous stress plus the modeled deviatoric component of the residual stress:

$$\tau^*_{ij} = \tau^v_{ij} - \tau^d_{ij} = 2(\nu + \nu_T) S_{ij}. \tag{13}$$

The bar notation denoting resolved variables $(\bar{u}_i, \overline{P})$ has been omitted for simplicity. The boundary integral term arises from the integration by parts and is only carried out over the portion of the domain without essential boundary conditions. Since the Galerkin method is unstable for the equal-order interpolations given above, we add additional stabilization terms which yields:

Find $\boldsymbol{u} \in \mathscr{S}_h^p$ and $P \in \mathscr{P}_h^p$ such that

$$B(w_i, q; u_i, P) = 0$$

$$B(w_i, q; u_i, P) = B_G(w_i, q; u_i, P) + \sum_{e=1}^{n_{el}} \int_{\widetilde{\Omega}_e} \{w_{i,j} \tau_M (u_j \mathscr{L}_i + u_i \mathscr{L}_j) + q_{,i} \tau_M \mathscr{L}_i + \tau_C w_{i,i} u_{j,j}\}\,\mathrm{d}x \tag{14}$$

for all $\boldsymbol{w} \in \mathscr{W}_h^p$ and $q \in \mathscr{P}_h^p$. Symbol $\widetilde{\Omega}_e$ denotes element interiors, excluding their closure. We have used $\mathscr{L}_i$ to represent the residual of the ith momentum equation,

$$\mathscr{L}_i = \dot{u}_i + (u_i u_j)_{,j} + P_{,i} - \tau^*_{ij,j} \tag{15}$$

The second line in the stabilized formulation, (14), represents streamline upwind/Petrov–Galerkin (SUPG) stabilization added to the Galerkin formulation of the compressible equations in conservation variables in the incompressible limit. As is shown in [6], this limit of the compressible equations in conservation variables $(\rho, \boldsymbol{u}, e_{\mathrm{tot}})$ under a change of variables to (p, u, T) is well-defined, leading to a conservative incompressible formulation. Variables e_{tot} and T are total energy and temperature, respectively.

The stabilization parameters for continuity and momentum are defined as given in [25],

$$\tau_M = \frac{1}{\sqrt{(2c_1/\Delta t)^2 + u_i g_{ij} u_j + c_2(\nu + \nu_T)^2 g_{ij} g_{ij}}}, \tag{16}$$

$$\tau_C = \frac{1/\tau_M}{\mathrm{tr}(g_{ij})}. \tag{17}$$

where c_2 is obtained based on the one-dimensional, linear advection–diffusion equation using a linear finite element basis and $g_{ij} = \xi_{k,i}\xi_{k,j}$ is the covariant metric tensor related to the mapping from global to element coordinates. The constant c_1 (associated to the temporal influence on the stabilization) is obtained by considering the local gradient in element space-time coordinate systems, as is done in [22]. However, for the purely spatial coordinate system used in our semi-discrete formulation, this constant is not well-defined. In this work we will study the dependence of simulation results on stabilization by varying c_1. Specifically, we will use c_1 as a parameter with which we will control dissipation due to stabilization making it weaker or stronger.

2.5. Numerical dissipation

Of importance in this section will be the numerical dissipation due to the SUPG stabilization, presented in the previous sub-section. Not much emphasis has been placed on this topic in past literature, and fur-

thermore, this is the first time (to the best of our knowledge) that a dissipation due to stabilization has been defined. Consider the filtered momentum equation in (2) where the term $[\overline{\tau_{ij}^v} - \tau_{ij}^d]_{,j}$ appears in the right hand side. In terms of molecular and eddy viscosities, this term can be expressed as

$$[\overline{\tau_{ij}^v} - \tau_{ij}^d]_{,j} = [2\nu\overline{S}_{ij} - (-2\nu_T\overline{S}_{ij})]_{,j}. \tag{18}$$

In deriving the weak form of the filtered equations, the previous term is brought to the left hand side and dotted by a weight function. The resulting term is integrated by parts resulting in a term of the form $w_{i,j}\{2\nu_T\overline{S}_{ij}\}$ in the integrand of the integral equation in (12). This can be seen by inserting τ_{ij}^* in (13) into the second line in (12). Note that in the Galerkin weak form in (12) the over-bar notation in $(\bar{u}_i, \overline{P})$ has been dropped for simplicity. The SUPG advection stabilization term of the integrand in (14) is of the form $w_{i,j}\{\tau_{ij}^{\mathrm{SUPG}}\}$, where

$$\tau_{ij}^{\mathrm{SUPG}} = \tau_M(\bar{u}_j\mathscr{L}_i + \bar{u}_i\mathscr{L}_j), \tag{19}$$

and $\mathscr{L}_i$ is given in (15). Again, the over-bar notation has been dropped in (15). Thus, analogous to physical SGS energy dissipation defined in Section 2.3 as $-2\nu_T\overline{S}_{ij}\overline{S}_{ij}$, we define SUPG (numerical) dissipation as $-\tau_{ij}^{\mathrm{SUPG}}\overline{S}_{ij}$. We would like to work with positive quantities, thus we denote

$$\epsilon_{\mathrm{SGS}} = 2\nu_T\overline{S}_{ij}\overline{S}_{ij} \quad \text{and} \quad \epsilon_{\mathrm{SUPG}} = \tau_{ij}^{\mathrm{SUPG}}\overline{S}_{ij} \tag{20}$$

as physical SGS dissipation and SUPG dissipation, respectively. To summarize, the definition of SUPG dissipation is motivated by looking at the Galerkin and SUPG terms of the weak formulation in (12) and (14), respectively. After integration by parts is performed while deriving the weak form, the stress τ_{ij}^* is multiplied by the gradient of the weight function which leads it to appear in the same form as the SUPG tensor $\tau_{ij}^{\mathrm{SUPG}}$. It is important to note that by considering the incompressible limit of the compressible stabilized formulation (leading to an incompressible formulation in conservative form), as discussed earlier, we are led to a symmetric SUPG tensor, a property also shared by τ_{ij}^*. If we had considered SUPG stabilization for the incompressible formulation in the advective form as is done in [25] and [28], our SUPG tensor and thereby our SUPG dissipation would have been more complicated to define due to the presence of extra stabilization terms.

A formal representation of numerical dissipation can be obtained by replacing w_i with u_i, taking u_i as zero over the entire boundary, and letting q be a constant in the weak form of the filtered equations in (12) and (14). In that case we obtain an equation for the resolved kinetic energy:

$$\begin{aligned}\int_\Omega \{\dot{k} + (\bar{u}_j k)_{,j}\}\,\mathrm{d}x = &\int_\Omega \{(-\bar{u}_j\overline{P} + \bar{u}_i\overline{\tau_{ij}^v} - \bar{u}_i\tau_{ij}^d)_{,j} - \overline{\tau_{ij}^v}\overline{S}_{ij} + \tau_{ij}^d\overline{S}_{ij}\}\,\mathrm{d}x \\ &- \sum_{n=1}^{n_{el}} \int_{\tilde{\Omega}_e} (\tau_{ij}^{\mathrm{SUPG}}\overline{S_{ij}} + \tau_C\bar{u}_{i,i}\bar{u}_{j,j})\,\mathrm{d}x.\end{aligned} \tag{21}$$

In obtaining (21), we have integrated by parts the advection and pressure terms as well as the viscous and SGS stress terms. The SUPG term was not integrated by parts, and has simply been re-expressed using the fact that $\tau_{ij}^{\mathrm{SUPG}}\bar{u}_{i,j} = \tau_{ij}^{\mathrm{SUPG}}\overline{S}_{ij}$ due to the symmetry of $\tau_{ij}^{\mathrm{SUPG}}$ and the non-symmetry of $\bar{u}_{i,j}$ (i.e. $\bar{u}_{i,j} \neq \bar{u}_{j,i}$). Notice that the integrands in (21) are exactly the terms in (9) except for an additional elemental quantity due to SUPG stabilization: $\tau_{ij}^{\mathrm{SUPG}}\overline{S_{ij}} + \tau_C\bar{u}_{i,i}\bar{u}_{j,j}$. The first term, $\tau_{ij}^{\mathrm{SUPG}}\overline{S_{ij}}$, is what earlier we denoted as SUPG dissipation. More precisely, this is dissipation due to SUPG advection stabilization. The second term, $\tau_C\bar{u}_{i,i}\bar{u}_{j,j}$, is dissipation due to SUPG continuity stabilization. For the wall-bounded turbulence problems studied here, this dissipation is negligible compared to the dissipation due to advection stabilization primarily because the latter is proportional to both the streamwise velocity and the wall-normal gradient of the streamwise velocity appearing in $\overline{S}_{ij}$:

$$\tau_{ij}^{\mathrm{SUPG}}\overline{S}_{ij} = \tau_M(\bar{u}_j\mathscr{L}_i + \bar{u}_i\mathscr{L}_j)\overline{S}_{ij}. \tag{22}$$

Regions far from walls have large freestream velocity while regions near walls have high wall-normal gradients of the velocity. Dissipation due to continuity stabilization is proportional to neither of these two, hence dissipation due to advection stabilization is dominant in all regions. In our computations we have observed that dissipation due to advection stabilization is 100 times or more greater than dissipation due to continuity stabilization, thus, the latter can be neglected from the overall SUPG dissipation. Herein we will consider SUPG dissipation due to advection stabilization only (i.e. $\epsilon_{\mathrm{SUPG}} = \tau_{ij}^{\mathrm{SUPG}}\overline{S}_{ij}$).

Furthermore, recalling that $\tau_{ij}^d = -2\nu_T\overline{S}_{ij}$ and inserting it into (21), we can denote $2\nu_T\overline{S}_{ij}\overline{S}_{ij}$ as subgrid-scale (SGS), physical dissipation as was done before. Substituting explicitly we see that (21) can be thought of as an integral statement of (9) plus numerical dissipation due to stabilization, viz.

$$\int_\Omega \{\dot{k} + (\bar{u}_j k)_{,j}\}\,\mathrm{d}x = \int_\Omega \{(-\bar{u}_j\overline{P} + \bar{u}_i\overline{\tau_{ij}^v} - \bar{u}_i\tau_{ij}^d)_{,j} - \epsilon_{\mathrm{MOL}} - \epsilon_{\mathrm{SGS}}\}\,\mathrm{d}x - \sum_{n=1}^{n_{el}}\int_{\tilde{\Omega}e}\epsilon_{\mathrm{SUPG}}\,\mathrm{d}x \tag{23}$$

where $\epsilon_{\mathrm{MOL}} = \overline{\tau_{ij}^v}\,\overline{S}_{ij}$. Note that if we apply the divergence theorem we see that

$$\int_\Omega \{\dot{k} + \epsilon_{\mathrm{MOL}} + \epsilon_{\mathrm{SGS}}\}\,\mathrm{d}x + \sum_{n=1}^{n_{el}}\int_{\tilde{\Omega}_e}\epsilon_{\mathrm{SUPG}}\,\mathrm{d}x + \int_\Gamma \{\bar{u}_j k + \bar{u}_j\overline{P} + \bar{u}_i\overline{\tau_{ij}^v} - \bar{u}_i\tau_{ij}^d\}n_j\,\mathrm{d}s = 0, \tag{24}$$

where n_j is the jth scalar component of the unit normal vector to the boundary Γ. If we have zero velocity boundary conditions on Γ then

$$\int_\Omega \{\dot{k} + \epsilon_{\mathrm{MOL}} + \epsilon_{\mathrm{SGS}}\}\,\mathrm{d}x + \sum_{n=1}^{n_{el}}\int_{\tilde{\Omega}_e}\epsilon_{\mathrm{SUPG}}\,\mathrm{d}x = 0 \tag{25}$$

from which we observe the three mechanisms of resolved kinetic energy decay: molecular, modeled and numerical. Most flows of interest do have some boundaries with non-zero velocities which provide a global production mechanism to the resolved kinetic energy.

3. Numerical results

In this section we will present simulation results of turbulent channel flow between parallel plates using the semi-discrete formulation previously introduced with piecewise tri-linear basis functions. Time integration is performed using the generalized-alpha method in [12].

The geometry of the problem, as sketched in Fig. 1, is composed of no-slip walls at $y = \pm h$ and periodicity in the spanwise (z-) and streamwise (x-)directions. Thus, the spanwise and streamwise directions are considered spatially homogeneous and the numerator and denominator in the dynamic model coefficient in (6) can be averaged over these directions. Most of the quantities presented throughout this work will be averaged over these homogeneous directions as well as in time, given that the flow is steady (homogeneous) in the temporal mean.

Simulations with Reynolds numbers, Re_τ, (based on the friction velocity, u_τ, and the channel half-width, h) at 180 and 395 were chosen for the purpose of having the benchmark direct numerical simulation results in [13] and [17] for comparison. By Dean's suggested correlation, as given in [13], $Re_\tau = 180$ corresponds to a bulk Reynolds number, Re, based on the bulk velocity and channel half-width of 2800. Similarly, $Re_\tau = 395$ corresponds to $Re = 6800$.

For the $Re_\tau = 180$ channel, $L_x = 4\pi h$ and $L_z = (4/3)\pi h$. The domain is represented by a hexahedral grid with 33 vertices in the streamwise (x-) and spanwise (z-)directions and 65 vertices in the direction normal to the walls (the y-direction). For the $Re_\tau = 395$ channel, $L_x = 2\pi h$ and $L_z = \pi h$. In this case, the hexahedral

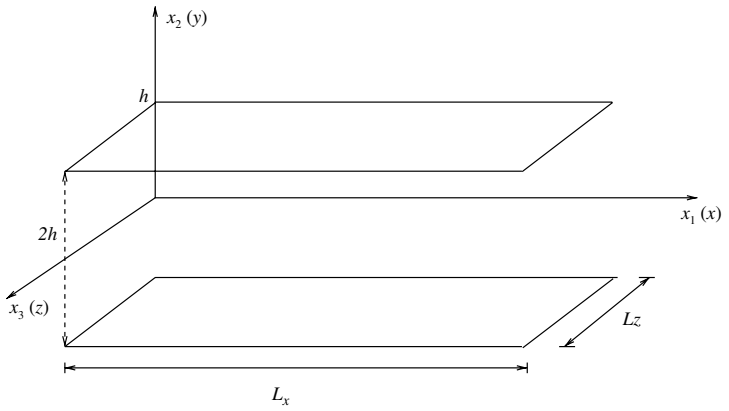

Fig. 1. Sketch of domain for channel flows.

grid has 33 vertices in the streamwise direction, 49 vertices in the spanwise direction and 65 vertices in the direction normal to the walls. For both channels, a stretching function is employed in the y-direction such that the first vertex off the wall is set at $\Delta y^+ = u_\tau \Delta y/\nu = 1$ away from the wall, where y is non-dimensionalized by h, and $\nu = 1/Re$. The $Re_\tau = 180$ channel simulations were made with a constant time step at 0.1 and the 395 channel simulations with a constant time step at 0.05. These time steps were chosen to satisfy the Courant, Friedrichs, Lewy (CFL) condition and maintain temporal accuracy.

3.1. Weak and strong dynamic models

As discussed earlier, we aim to vary the strength of SUPG stabilization through the parameter associated with the temporal portion of the intrinsic time scale τ_M. We also aim to vary the strength of the dynamic model. To that extent, we change the width of the test filter used in the dynamic model computation. Although we do not go into much detail on these test filters, it turns out that if the width of the test filter is sufficiently large, the influence of the dynamic model away from the core turbulence, approaching the walls, is weaker, as shown in [26]. Thus, the wider the test filter, the weaker the model. We use two three-dimensional test filters referred to as the standard filter and as the wide filter. The standard filter is obtained by approximating the generalized box filter (a filter that takes on the value of one over the volume of the elements surrounding a given node for the very same elements and zero outside of this collection of elements, details discussed in [27]) while the wide filter is obtained by approximating the generalized box filter applied twice. The standard filter will be referred to as S1 and the wide filter as W1, given that both filters are obtained with one-point Gaussian quadrature approximation of the generalized box filter. The filter width ratio parameter appearing in the dynamic model in (8) is taken as $\alpha = 3$ when filter S1 is used and is taken as $\alpha = 9$ when filter W1 is used. A complete description of these filters and how to compute their widths is given [27].

3.2. A modification to the dynamic model based on SUPG

In this section we will present simulation results with the wall-resolved channel flow at $R_\tau = 180$. Our goal is to understand the behavior of the dynamic model (physical) SGS dissipation in the presence of SUPG (numerical) dissipation and vice-versa. We begin by looking at Fig. 2, where we show the components of the SUPG tensor, $\tau_{ij}^{\mathrm{SUPG}}$, averaged over spatially homogeneous directions and over time for simulations with different combinations of SUPG stabilization and dynamic model. We present the four

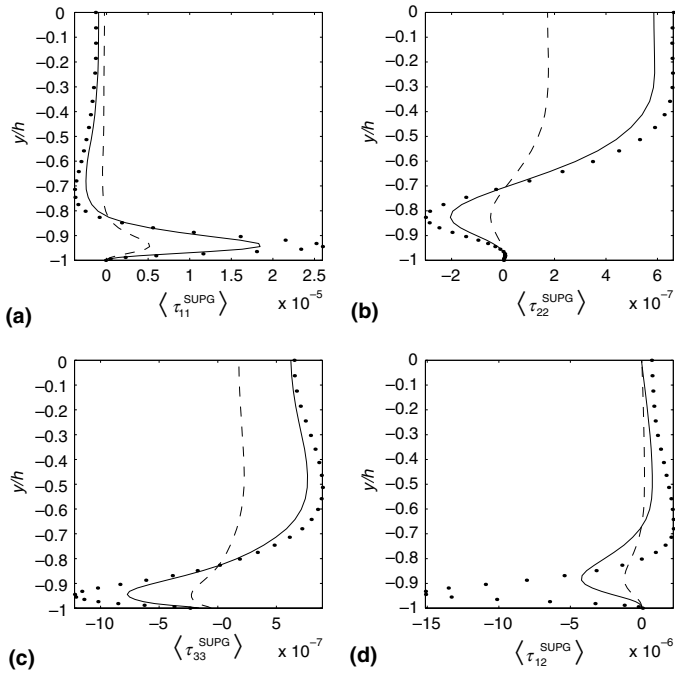

Fig. 2. Components of the SUPG tensor $\tau_{ij}^{\mathrm{SUPG}}$. (—): $c_1 = 16$ (strong SUPG) and strong dynamic model; (---): $c_1 = 64$ (weak SUPG) and strong model; (●): $c_1 = 16$ (strong SUPG) and weak model.

non-zero (in the mean) components of the SUPG tensor. Notice that $\tau_{11}^{\mathrm{SUPG}}$ and $\tau_{12}^{\mathrm{SUPG}}$ are dominant over $\tau_{22}^{\mathrm{SUPG}}$ and $\tau_{33}^{\mathrm{SUPG}}$. Although not shown, all components are symmetric about the channel centerline at $y/h = 0$, except for $\tau_{12}^{\mathrm{SUPG}}$, which is anti-symmetric.

The influence of the SUPG stabilization decreases as constant c_1 is increased, as expected from looking at the expression for τ_M in (16). We also change the strength of the dynamic model by changing the width of the test filter. From Fig. 2, we see that by switching the dynamic model from strong to weak while leaving c_1 unchanged, the peaks of the SUPG tensors increase in magnitude to account for lack of physical SGS energy dissipation. SUPG stabilization seems to be at least partially adjusting to the strength of the model. The previous conclusions can be drawn as well from Fig. 3a, where we show SUPG dissipation in wall units. Note that for the first five planes of vertices off the walls, SUPG dissipation is negative. In Fig. 3b we see that the weaker model near the wall gives rise to smaller physical SGS dissipation in this region.

Of great importance, as seen in Fig. 3b, is that keeping the model fixed and changing the influence of SUPG stabilization by varying c_1 between 16 and 64, does not seem to effect physical SGS dissipation by much. However, looking at Fig. 4, we see that actually there is some adjustment of the eddy viscosity when keeping the model fixed and varying the SUPG strength. A strong SUPG gives rise to a lower eddy viscosity. The reason for this can be explained by first recalling the eddy viscosity as

$$\nu_T = (C_s\overline{\Delta})^2 \mid \overline{S} \mid. \tag{26}$$

A strong SUPG leads to a less energetic flow due to higher numerical dissipation. In turn, a less energetic flow leads to lower values of the norm of the filtered strain-rate tensor ($\mid \overline{S} \mid$), appearing in (26), thus a lower eddy viscosity. However, this adjustment of the physical model to a stronger SUPG is not enough as evinced by the time history of the force exerted by the flow on the channel walls, shown in Fig. 5a. In this figure we see that increasing SUPG, slightly decreases the wall force. Although the physical SGS model

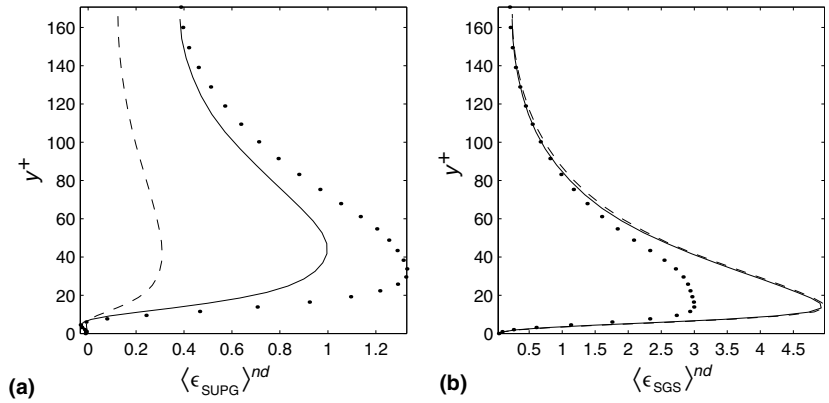

Fig. 3. Non-dimensionalized dissipations, $\langle \epsilon \rangle^{nd} = \langle \epsilon \rangle h/u_\tau^3$. (a) SUPG dissipation on the left and (b) dynamic model/SGS dissipation on the right. (—): $c_1 = 16$ (strong SUPG) and strong model; (---): $c_1 = 64$ (weak SUPG) and strong model; (●): $c_1 = 16$ (strong SUPG) and weak model.

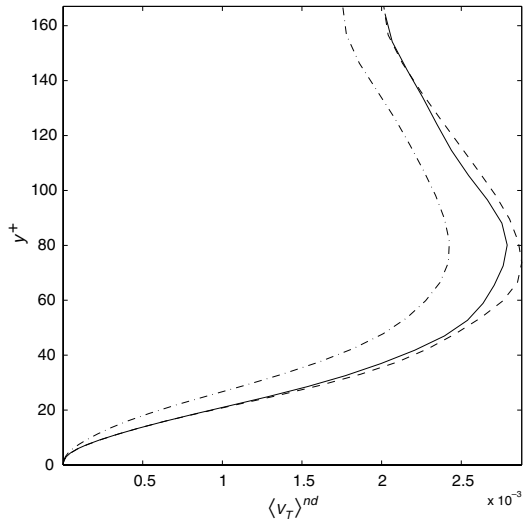

Fig. 4. Non-dimensionalized eddy viscosity. $\langle v_T \rangle^{nd} = \langle v_T \rangle/(u_\tau h)$, where u_τ is the computed friction velocity. (—): $c_1 = 16$ and strong model; (---): $c_1 = 64$ (weak SUPG) and strong model.

weakens to account for the stronger SUPG stabilization, this adjustment is not enough to keep the mean wall force the same between both simulations. The reason for this is that even though there is an adjustment of the eddy viscosity through the filtered strain-rate tensor, there is hardly any adjustment at all by the physical model coefficient $(C_s\overline{\Delta})^2$, as seen in Fig. 6. A possible reason for the non-adjusting nature of the physical model is that the model coefficient is computed based on sampling larger resolved components of the flow than those believed to be affected by SUPG stabilization. Changing SUPG stabilization does not greatly affect the larger resolved components used in computing the model coefficient, consequently leaving it relatively unchanged.

As mentioned earlier, the wide filter W1, leads to lower values of the dynamic model coefficient, which reflects through much higher wall forces due to a more energetic flow. This can be seen by comparing the

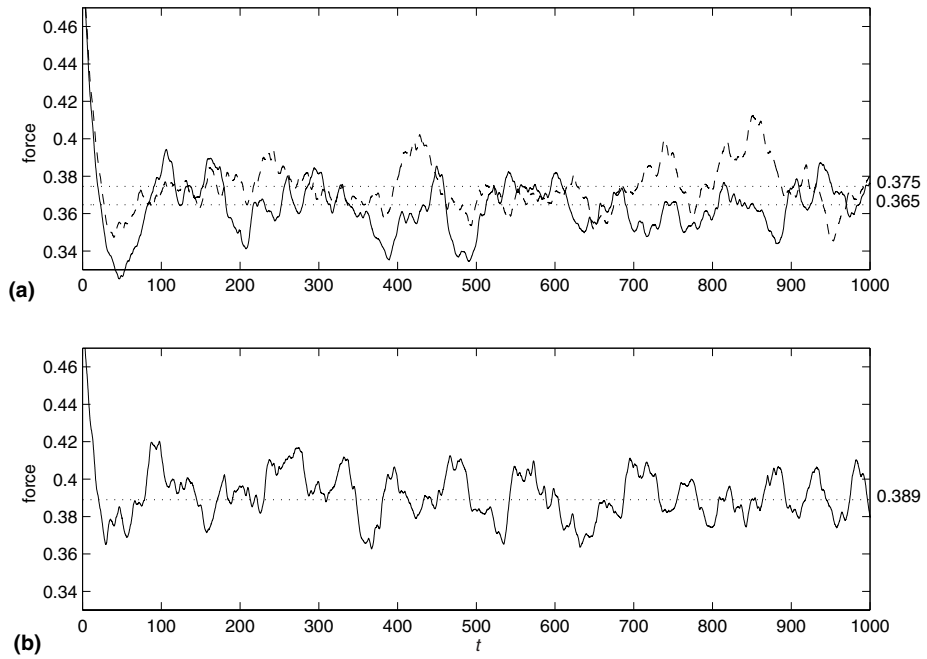

Fig. 5. (a) Force histories with strong model and with varying SUPG. (—): $c_1 = 16$ (strong SUPG); (- - -): $c_1 = 64$ (weak SUPG). (b) Force history with weak model and with $c_1 = 16$ in the stabilization (strong SUPG). The mean wall force should be approximately 0.435.

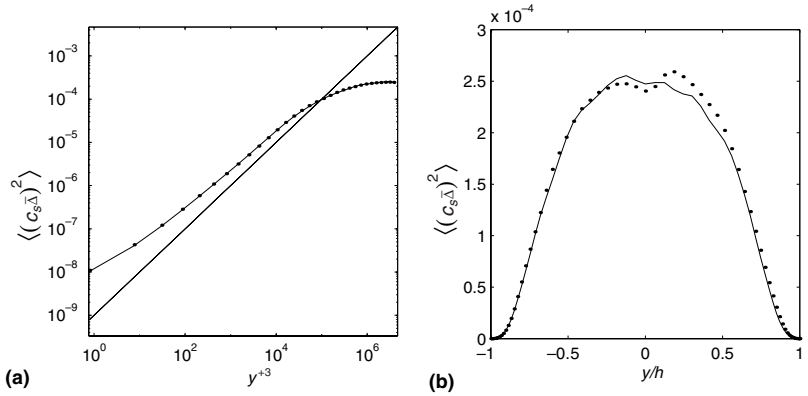

Fig. 6. (a) Dynamic model coefficient versus y^{+3}. (b) Dynamic model coefficient versus y. For (a) and (b), (—): strong model and $c_1 = 16$ (strong SUPG); (●): strong model and $c_1 = 64$ (weak SUPG). The solid straight line denotes a y^{+3} profile.

solid curves in Fig. 5a and 5b. Here, SUPG is not able to adjust enough so as to keep the forces the same between the two cases.

Here, we aim to modify the physical model such that at least when keeping the filter fixed and changing the SUPG strength, the model can adjust enough to retain nearly the same mean wall force which, from experience, is a global indicator of the total dissipation. If we presume the dynamic model to be capable of predicting the correct level of dissipation then it makes sense to define a correction which "discounts"

the dissipation present in the numerical method. We propose to account for SUPG stabilization in the physical SGS dynamic model at the energy dissipation level by setting the new, corrected physical SGS dissipation to be

$$\epsilon^*_{\mathrm{SGS}} = \epsilon_{\mathrm{SGS}} - \epsilon_{\mathrm{SUPG}} \equiv 2\nu_T \overline{S}_{ij}\overline{S}_{ij} - \tau^{\mathrm{SUPG}}_{ij}\overline{S}_{ij}. \tag{27}$$

The previous corrected physical SGS dissipation implies a corrected eddy viscosity (ν^*_T), thus a corrected dynamic model coefficient $(C_s\overline{\Delta})^{*2}$. The corrected eddy viscosity and model coefficient are related as

$$\epsilon^*_{\mathrm{SGS}} = 2\nu^*_T \overline{S}_{ij}\overline{S}_{ij} = 2(C_s\overline{\Delta})^{*2} \mid \overline{S} \mid \overline{S}_{ij}\overline{S}_{ij}, \tag{28}$$

where the first equality follows from our definition of physical SGS dissipation in (20), and the second equality follows from the modeled eddy viscosity in (26). Recalling the corrected physical SGS dissipation in (27) and making use of the fact that $\mid \overline{S}\mid^2 = 2\overline{S}_{ij}\overline{S}_{ij}$, we can solve for the corrected dynamic model coefficient from (28) as

$$(C_s\overline{\Delta})^{*2} = \frac{\epsilon^*_{\mathrm{SGS}}}{\mid \overline{S}\mid^3} = \frac{2\nu_T \overline{S}_{ij}\overline{S}_{ij} - \tau^{\mathrm{SUPG}}_{ij}\overline{S}_{ij}}{\mid \overline{S}\mid^3}. \tag{29}$$

In terms of the original model coefficient, $(C_s\overline{\Delta})^2$ we have

$$(C_s\overline{\Delta})^{*2} = \frac{\epsilon^*_{\mathrm{SGS}}}{\mid \overline{S}\mid^3} = \frac{(C_s\overline{\Delta})^2 \mid \overline{S}\mid^3 - \tau^{\mathrm{SUPG}}_{ij}\overline{S}_{ij}}{\mid \overline{S}\mid^3}. \tag{30}$$

An alternate interpretation of this approach is obtained by dividing (30) by $(C_s\overline{\Delta})^2$ to obtain a "correction factor", ϕ, for $(C_s\overline{\Delta})^2$ (and thus ν_T), viz.

$$\phi = \frac{(C_s\overline{\Delta})^{*2}}{(C_s\overline{\Delta})^2} = 1 - \frac{\tau^{\mathrm{SUPG}}_{ij}\overline{S}_{ij}}{(C_s\overline{\Delta})^2 \mid \overline{S}\mid^3} = 1 - \frac{\epsilon_{\mathrm{SUPG}}}{\epsilon_{\mathrm{SGS}}}. \tag{31}$$

For stability purposes, the numerator and denominator in (29) or (30) are averaged over spatially homogeneous directions of the flow, analogous to the averaging performed for the uncorrected, classical dynamic model coefficient. In practice, if the spatially averaged SUPG dissipation is negative, such as is the case for the first few planes off the walls, the SUPG correction is not made and the classical dynamic model is left unmodified. The corrected eddy viscosity is obtained as

$$\nu^*_T = (C_s\overline{\Delta})^{*2} \mid \overline{S} \mid. \tag{32}$$

In view of this corrected eddy viscosity, the reader might be led to think that we are changing the partial differential equations we are solving to account for the numerical method. However, we note that by modifying the eddy viscosity, we are not changing the partial differential equations in ways different than any other model change/choice would. We are simply modifying the classical model approximating the subgrid-scale (residual) stress present in the filtered Navier–Stokes equations. There are different reasons for changing or modifying the model approximating the subgrid-scale stress. Historically, changes or modifications to the Smagorinsky model have been made to better account for the physics of the turbulence. Here we have proposed a modification to better account for the numerical aspect of the solution, insuring that the aggregate behavior is more faithfully modeled.

Furthermore, our modification to the eddy viscosity of the dynamic model retains the residual structure of the equations because it is strictly dependent on the amount of SUPG stabilization. As the numerical solution becomes more accurate, SUPG stabilization vanishes; consequently, our modification vanishes as well. The corrected model coefficient in (29) leading to the corrected eddy viscosity in (32) is motivated from the result that the uncorrected dynamic model does not seem to be aware of numerical dissipation,

mostly due to an unaffected model coefficient. In the case were $\epsilon_{\mathrm{SUPG}} \ll \epsilon_{\mathrm{SGS}}$, the correction to the SGS physical dissipation becomes negligible (which can be seen by inspecting (31)), essentially leading to the usual dynamic model. However, if these two dissipations are of the same order, the modification has a stronger impact. Regardless of the difference between physical SGS and numerical SUPG dissipations, the total subgrid dissipation will always be due to the physical SGS model alone and not due to SUPG since

$$\text{total subgrid dissipation} = \epsilon^{*}_{\mathrm{SGS}} + \epsilon_{\mathrm{SUPG}} = \epsilon_{\mathrm{SGS}}. \tag{33}$$

This can be seen by substituting $\epsilon^{*}_{\mathrm{SGS}}$ given by the first equality in (27) into (33). Hence, as a result of the modification in (27), SUPG stabilization is used for stabilization purposes only. This is a desirable feature since in principle, numerical dissipation should not interfere with subgrid dissipation meant to be provided by the physical SGS model only.

Other ways of accounting for the presence of SUPG stabilization can be studied. For example, one may consider the SUPG tensor $\tau^{\mathrm{SUPG}}_{ij}$ as a true (physical) stress and include it as an extra SGS stress in the derivation of the dynamic model. However, from a physical point of view this is not appropriate because the components of $\tau^{\mathrm{SUPG}}_{ij}$ do not behave like those of a true (physical) stress. For example, the components of $\tau^{\mathrm{SUPG}}_{ij}$ change sign throughout the lower part of the channel (see Fig. 2), uncharacteristic of a true stress. Furthermore, it is also worth pointing out that many researchers have tested the Smagorinsky model using direct numerical simulation databases (see Ref. [7] and references within). All have indicated that the model does not possess high correlation with the exact SGS stress, but possesses high correlation with the divergence of the exact SGS stress and an even much better correlation with the exact SGS energy dissipation. This may suggest one reason why it is more appropriate to account for SUPG stabilization based on energy dissipation rather than on stress.

4. Turbulent channel LES with the SUPG-modified dynamic model

In the up-coming sub-sections we will see the effect of the corrected or modified dynamic model coefficient in (30) on simulation results of wall-resolved turbulent channel flow. Specifically, we will study the effect of SUPG correction in three cases distinguished by the difference between SUPG and SGS dissipation. In the first case, we will study SUPG correction in the $Re_\tau = 180$ channel with the dynamic models using filter S1. In the second case we perform simulations of the $Re_\tau = 180$ with the models using filter W1. In the second case, with filter W1, the difference between peak SGS dissipation and SUPG dissipation is less than in first case with filter S1. In the third case, we perform simulations of an $Re_\tau = 395$ channel flow with dynamic models using filter S1. For this case the peak difference in SGS and SUPG dissipations is slightly greater than in the first case. It will be seen than when the difference between peak SGS and SUPG dissipations is low, the model correction introduced in (27) can play an important role.

4.1. Channel flow at $Re_\tau = 180$ with strong model

Here we study cases in the channel at $Re_\tau = 180$ for which the corrected and non-corrected dynamic models are computed using filter S1 under different strengths of the SUPG stabilization. We begin by looking at Fig. 7. Comparing the curves with $c_1 = 64$, we see that when SUPG correction is employed, the magnitude of the components of the SUPG tensor are higher due to the reduction of the dynamic model coefficient. In other words, the magnitude of the components of the SUPG tensor increase due to a more energetic flow resulting from a lower eddy viscosity given by a corrected dynamic model. This is more noticeable in the case of strong SUPG dissipation (when $c_1 = 16$). Furthermore, the adjustment of the model due to a change in SUPG strength is much more pronounced as seen in the plots of SGS energy dissipations and viscosities in Figs. 8b and 9, respectively.

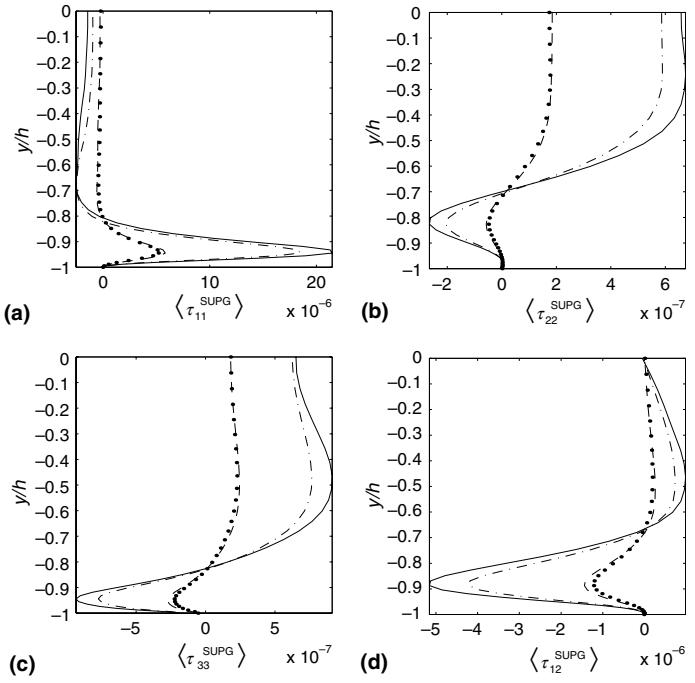

Fig. 7. Components of the SUPG tensor $\tau_{ij}^{\mathrm{SUPG}}$ with and without SUPG correction in the dynamic model with filter S1. (—): $c_1 = 16$ and SUPG correction; (---): $c_1 = 64$ and SUPG correction. (– · –): $c_1 = 16$ and no SUPG correction; (●): $c_1 = 64$ and no SUPG correction.

As expected, the SUPG correction introduces lesser changes in the cases for which SUPG is weak corresponding to $c_1 = 64$. The reason for this is that when $c_1 = 64$, ϵ_{SUPG} is much smaller than when $c_1 = 16$, hence it does not affect $\epsilon^*_{\mathrm{SUPG}}$ in (27) as much. This can be clearly seen by comparing mean wall forces (Fig. 10) and SGS dissipations (Fig. 8b) in the corrected and uncorrected model cases under weak SUPG.

In Fig. 10 we plot time histories of the forces on the channel walls with and without SUPG correction. Notice that when the dynamic model does not have SUPG correction, corresponding to Fig. 10a, the peaks and troughs of the force recorded with $c_1 = 16$ are lower than those of the force with $c_1 = 64$. The relative difference between the two mean forces, defined as $(f_{\mathrm{high}} - f_{\mathrm{low}})/f_{\mathrm{low}}$, is 3%. In this case, as c_1 goes from 16 to 64, SUPG dissipation decreases while SGS dissipation remains nominally the same, giving rise to a more energetic flow, and consequently a higher wall force. When the dynamic model does have SUPG correction, corresponding to Fig. 10b, the model adjusts to the change in SUPG stabilization, giving rise to more similar force histories for which the relative mean difference is 1%.

4.2. Channel flow at $Re_\tau = 180$ with weak model

In this sub-section we study cases in the channel at $Re_\tau = 180$ for which the corrected and non-corrected dynamic model are computed using wide filter W1 under different strengths of the SUPG stabilization.

Looking at Fig. 11 we see that once again the magnitude of the components of the SUPG tensor increase due to a more energetic flow resulting from a lower eddy viscosity given by a corrected dynamic model. This is more noticeable in the case of strong SUPG dissipation (when $c_1 = 16$). Furthermore, with SUPG correction the adjustment of the model due to a change in SUPG strength is greater as seen in the plots of SGS energy dissipations and viscosities in Figs. 12b and 13, respectively. Similar to the case presented in

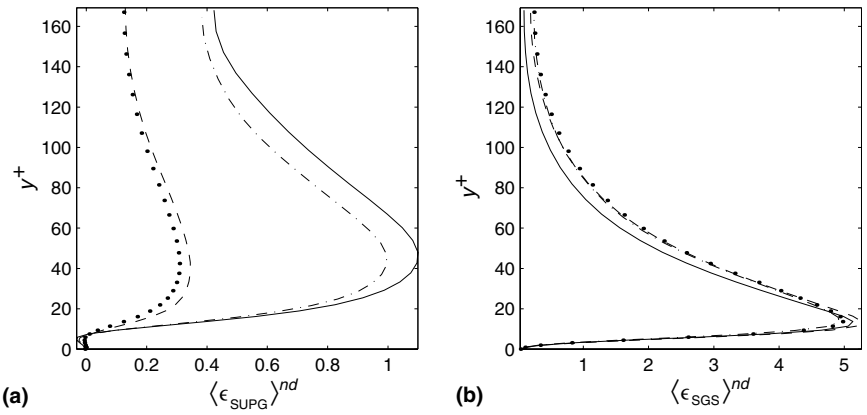

Fig. 8. Non-dimensionalized dissipations. (a) SUPG dissipation on the left and (b) dynamic model/SGS dissipation on the right. Here results are with and without SUPG correction in the dynamic model with filter S1. (—): $c_1 = 16$ and SUPG correction; (---): $c_1 = 64$ and SUPG correction. (– · –): $c_1 = 16$ and no SUPG correction; (●): $c_1 = 64$ and no SUPG correction.

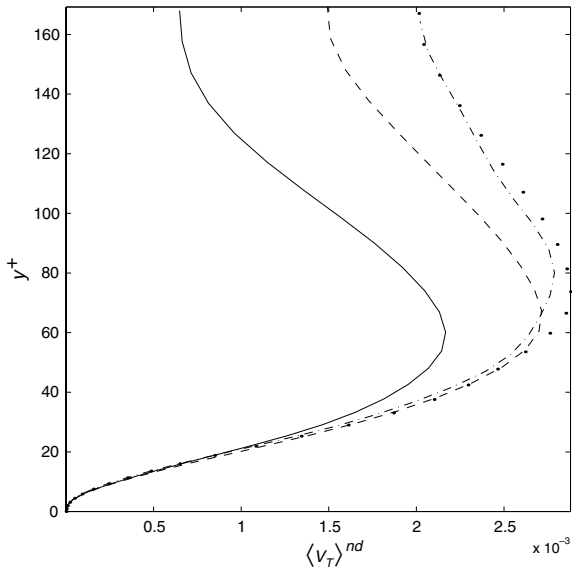

Fig. 9. Non-dimensionalized eddy viscosity with and without SUPG correction in the dynamic model with filter S1. (—): $c_1 = 16$ and SUPG correction; (---): $c_1 = 64$ and SUPG correction. (– · –): $c_1 = 16$ and no SUPG correction; (●): $c_1 = 64$ and no SUPG correction.

the previous sub-section, the SUPG correction introduces lesser changes in the cases for which SUPG is weak corresponding to $c_1 = 64$.

In Fig. 14 we plot wall force histories for when the model is corrected and uncorrected. Once again, the uncorrected model leads to a lower mean force when the SUPG stabilization is increased. On the other hand, the corrected model keeps the mean wall force constant under changes of SUPG strength. Prior to SUPG correction, the relative mean difference in the forces is 6 percent, and after SUPG correction the difference is negligible.

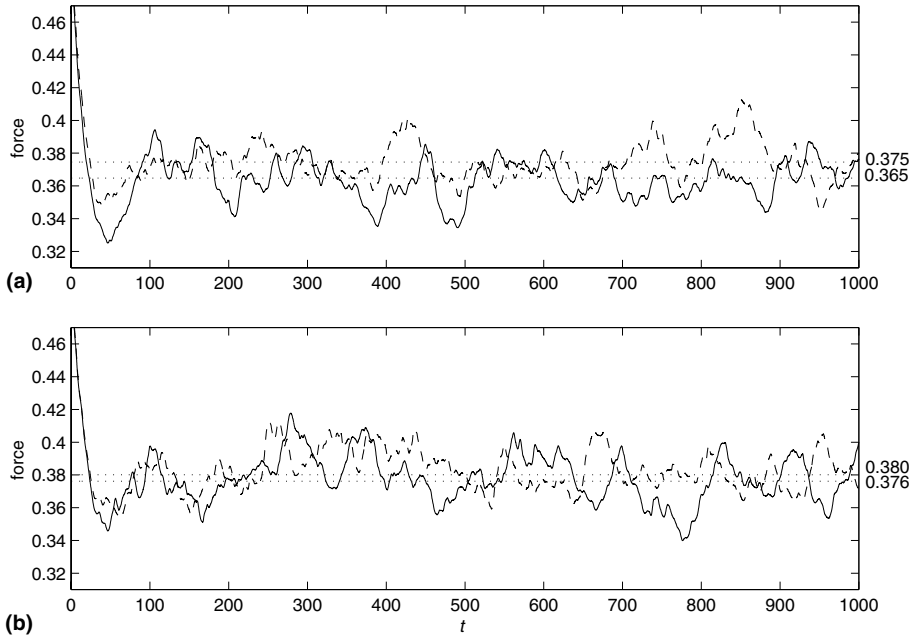

Fig. 10. (a) Wall forces without SUPG correction on the top and (b) wall forces with SUPG correction on the bottom. In all cases the model was computed with filter S1. (—): $c_1 = 16$; (---): $c_1 = 64$.

It is important to note that for the cases considered in this sub-section that have strong SUPG stabilization, the peak SGS dissipation is approximately two times greater than the peak SUPG dissipation. In the previous sub-section, for the case of strong stabilization, the peak SGS dissipation is approximately five times greater than the peak SUPG dissipation. In the scenario of relatively small difference between the strengths of SGS and SUPG dissipations, the dynamic model correction is seen to have a greater impact on the results than in cases when the maximum difference between SGS and SUPG dissipations is greater. This can be seen by comparing the mean wall force between the corrected and uncorrected models under high difference between maximum SGS and SUPG dissipations (Fig. 10) and under low difference between these two (Fig. 14). In Fig. 10, the difference in the force histories caused by changing the SUPG strength is less pronounced than in Fig. 14. Thus, having a corrected dynamic model proves to be more significant in cases were the SGS and the SUPG dissipations are of comparable size.

Next, in Figs. 15–17 we compare mean streamwise velocity, root-mean-square (rms) of velocity fluctuations and Reynolds stress between strong and weak dynamic models with and without SUPG correction. For all cases SUPG dissipation is strong at $c_1 = 16$. In the case of the weak dynamic model, which uses filter W1, the SUPG correction introduces greater changes, especially in terms of mean streamwise velocity and Reynolds stress component $\langle u_1' u_2' \rangle$. This is due to the small difference between SGS and SUPG energy dissipation. From these figures we can clearly say that the dynamic model with SUPG correction using test filter W1 is the top performer, which can be directly attributed to its better approximation of the mean wall force.

4.3. Channel flow at $Re_\tau = 395$ with strong model

As the Reynolds number increases, more is required from the SGS and the SUPG models. In this section we consider turbulent channel flow at $Re_\tau = 395$ with the dynamic model using filter S1. By Dean's suggested

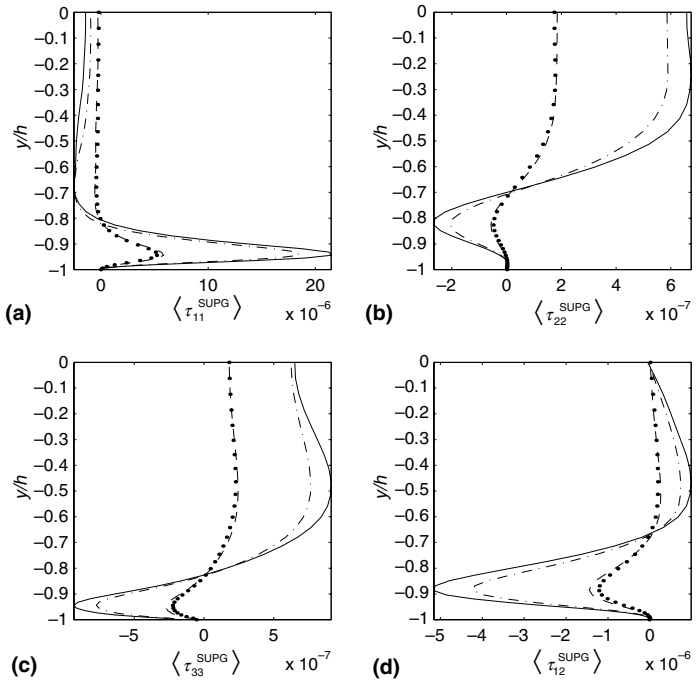

Fig. 11. Components of the SUPG tensor τ_{ij}^{SUPG} with and without SUPG correction in the dynamic model with the filter W1. (—): $c_1 = 16$ and SUPG correction; (---): $c_1 = 64$ and SUPG correction. (– · –): $c_1 = 16$ and no SUPG correction; (●): $c_1 = 64$ and no SUPG correction.

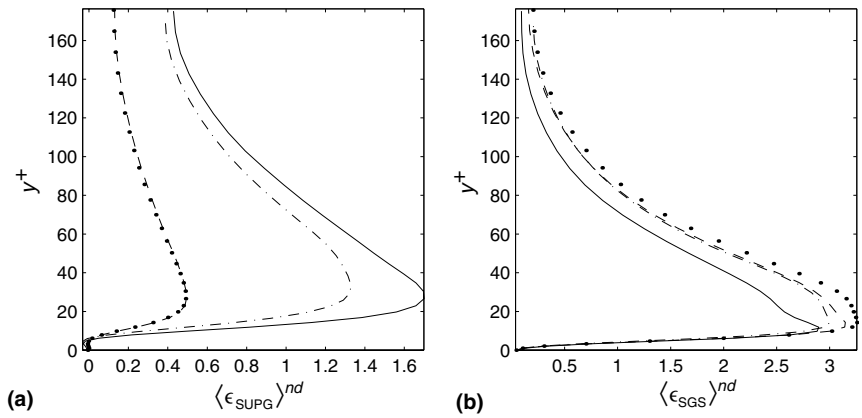

Fig. 12. Non-dimensionalized dissipations. (a) SUPG dissipation on the left and (b) dynamic model/SGS dissipation on the right. Here results are with and without SUPG correction in the dynamic model with filter W1. (—): $c_1 = 16$ and SUPG correction; (---): $c_1 = 64$ and SUPG correction. (– · –): $c_1 = 16$ and no SUPG correction; (●): $c_1 = 64$ and no SUPG correction.

correlation, as given in [13], $Re_\tau = 395$ corresponds to a bulk Reynolds number, Re, based on the bulk velocity and channel half-width of 6800. Referring back to Fig. 1c, for this problem $L_x = 2\pi h$ and $L_z = \pi h$. Here, the domain is split by 33 vertices in the streamwise direction, 49 vertices in the spanwise direction and 65 vertices in the direction normal to the walls. Similar to the wall-resolved channel flow at $Re_\tau = 180$, a hyper-

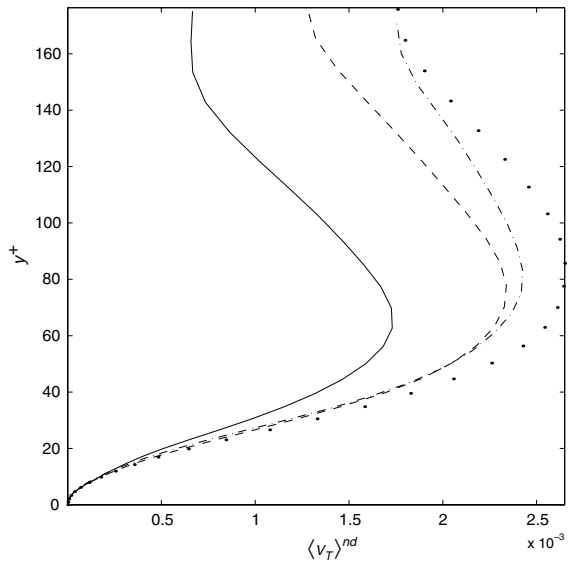

Fig. 13. Non-dimensionalized eddy viscosity with and without SUPG correction in the dynamic model with filter W1. (—): $c_1 = 16$ and SUPG correction; (- - -): $c_1 = 64$ and SUPG correction. (– · –): $c_1 = 16$ and no SUPG correction; (●): $c_1 = 64$ and no SUPG correction.

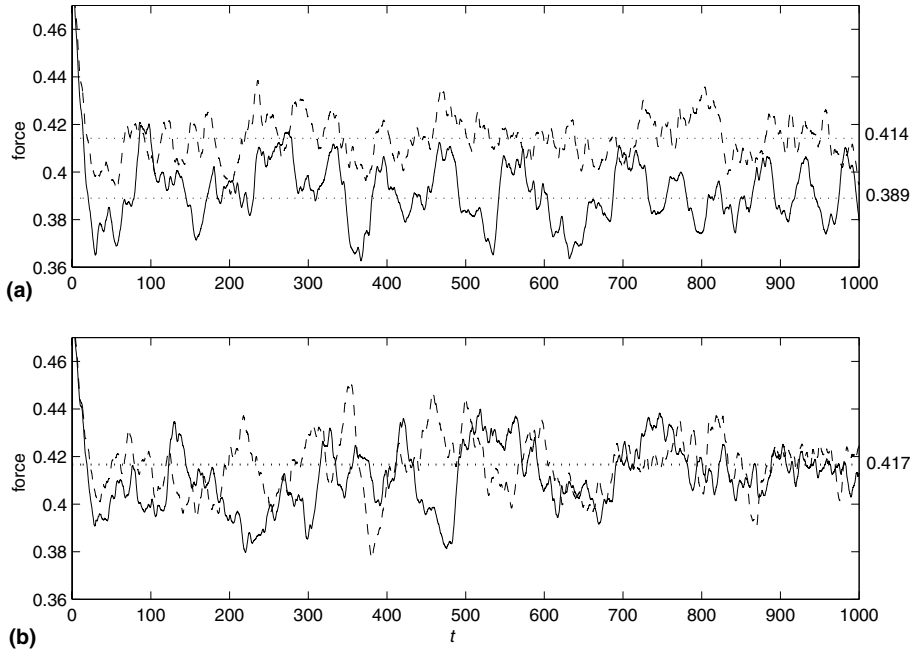

Fig. 14. (a) Wall forces without SUPG correction on the top and (b) wall forces with SUPG correction on the bottom. In all cases the model was computed with filter W1. (—): $c_1 = 16$; (- - -): $c_1 = 64$.

bolic stretching function is employed in the y-direction such that the first vertex off the wall is set at a distance $\Delta y^+ = u_\tau \Delta\, y/\nu = 1$ away from the wall, where y is non-dimensionalized by h, and $\nu = 1/Re$.

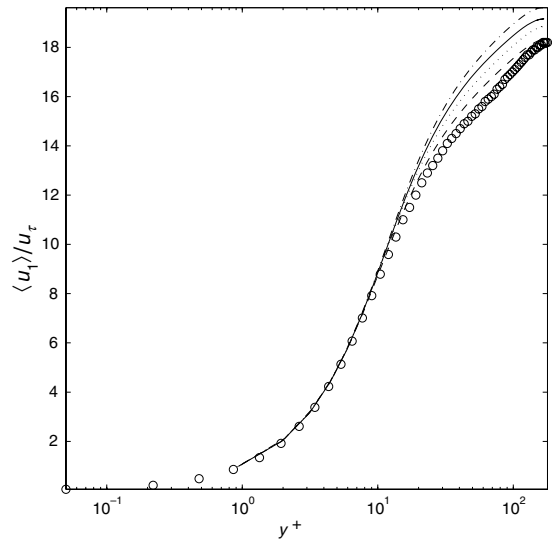

Fig. 15. Mean streamwise velocity in wall coordinates with dynamic model using filter S1 and SUPG correction (—), filter W1 and SUPG correction (---), filter S1 and no SUPG correction (– · –), and filter W1 and no SUPG correction (●). (○): mean velocity in the DNS in [13].

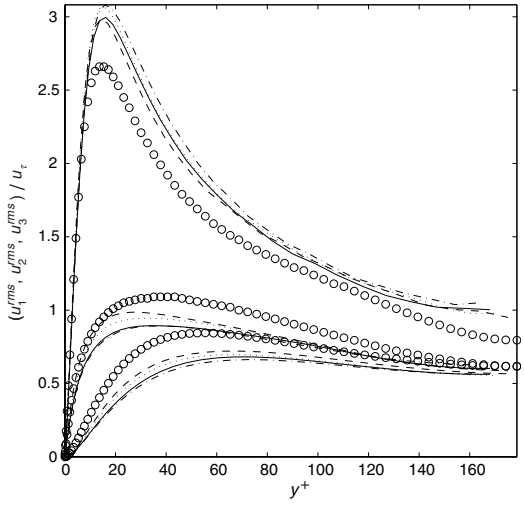

Fig. 16. Rms of velocity fluctuations in wall coordinates. Rms of velocities with dynamic model using filter S1 and SUPG correction (—), filter W1 and SUPG correction (---), filter S1 and no SUPG correction (– · –), and filter W1 and no SUPG correction (●). (○): rms of fluctuations in the DNS in [13].

Due to the more energetic nature of this flow compared to the flow at $Re_\tau = 180$, the dynamic model is expected to cause stronger SGS dissipations. SUPG dissipation is also greater in the current flow compared to the $Re_\tau = 180$ case. With an uncorrected model, the maximum SGS dissipation is approximately five and one-half times greater than then maximum SUPG dissipation. This difference is slightly greater than that studied in sub-section 6.3.1, in which the factor was approximately five. Given previous results, one would expect for the corrected dynamic model to impact results less than it did in earlier simulations.

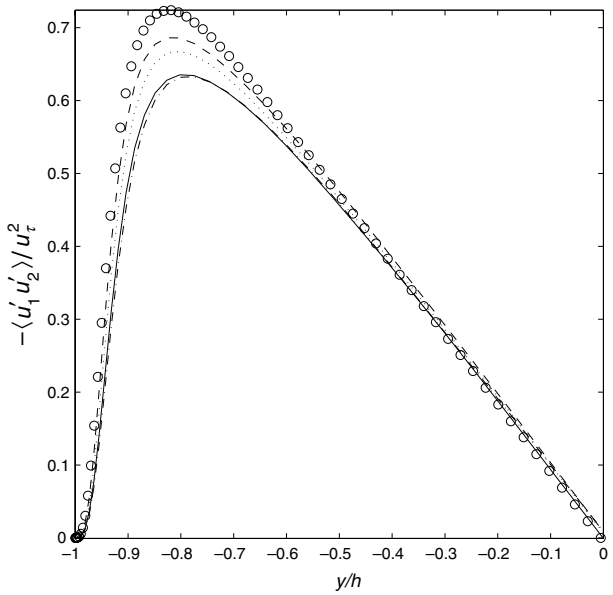

Fig. 17. Reynolds stress component $\langle u_1' u_2' \rangle$ with dynamic model using using filter S1 and SUPG correction (—), filter W1 and SUPG correction (- - -), filter S1 and no SUPG correction (– · –), and filter W1 and no SUPG correction (●). (○): Reynolds stress component in the DNS in [13].

In Figs. 18 and 19, we plot the SUPG tensor and dissipations due to SGS and SUPG. Looking at the SGS dissipation, the corrected dynamic model does not adjust as much as in earlier cases. This is further evinced by looking at the mean forces in Fig. 20. As seen in this figure, the mean forces in the uncorrected model cases do not differ by much (especially in the last third of the simulations) as the strength of SUPG stabilization is changed. Over the last third of the simulations, the mean forces differ by less than 2 percent. The SUPG corrected dynamic model brings them even closer.

The same trends observed in the $Re_\tau = 180$ channel simulations were observed for the $Re_\tau = 395$ channel simulations in terms of mean velocity, root mean square velocity, and the Reynolds stress. The improvement brought about by the modified dynamic model in terms of these quantities is hardly noticeable, which is why we do not include these results here. As discussed earlier, the minimal improvement brought by the modified dynamic model in the $Re_\tau = 395$ cases was expected because, by construction, the modification becomes negligible for cases where the ratio of physical dissipation to SUPG (numerical) dissipation is high.

5. Final remarks

In this article we have presented a modification to the Smagorinsky dynamic subgrid-scale stress model for the purpose of allowing the model to adjust itself in the presence of varying numerical dissipation due to SUPG stabilization. The success of the SUPG modification was shown on LES of turbulent channel flows with Reynolds numbers, Re_τ, of 180 and 395. It was concluded that for cases when the maximum difference between SGS and SUPG dissipation is low, the modification to the model plays an important role in allowing the model to adjust properly under different amounts of SUPG dissipation. In cases were this difference

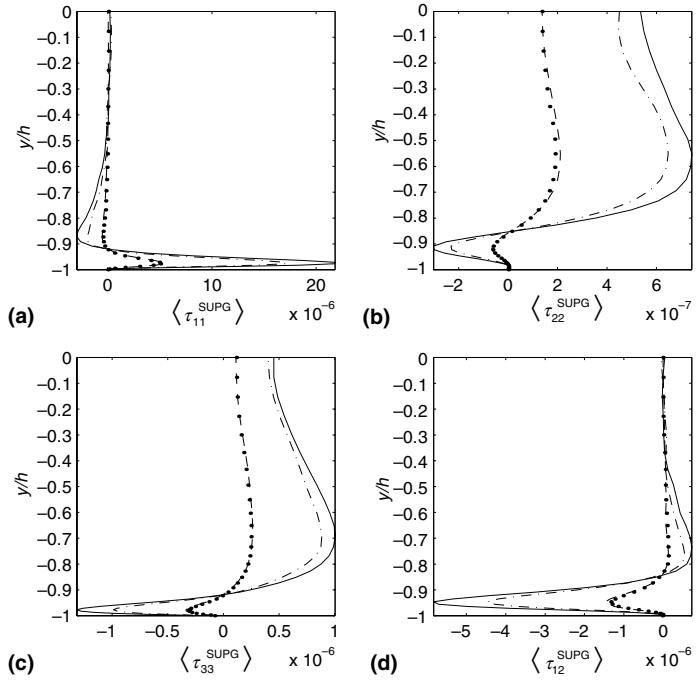

Fig. 18. Components of the SUPG tensor $\tau_{ij}^{\mathrm{SUPG}}$ with and without SUPG correction in the dynamic model with filter S1. (—): $c_1 = 16$ and SUPG correction; (---): $c_1 = 64$ and SUPG correction. (– · –): $c_1 = 16$ and no SUPG correction; (●): $c_1 = 64$ and no SUPG correction.

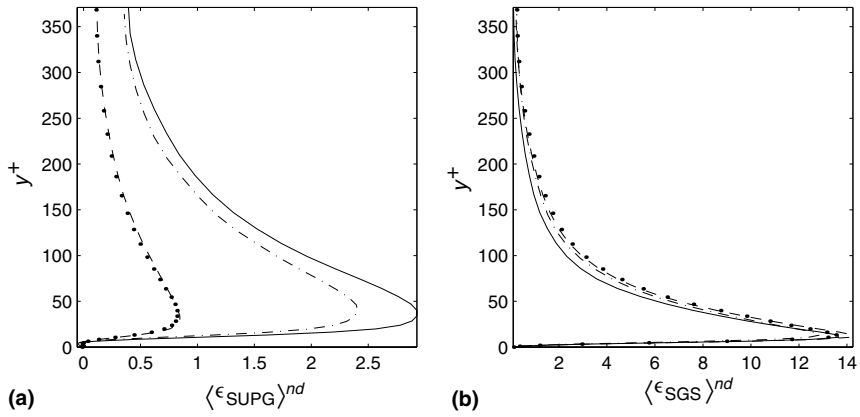

Fig. 19. Non-dimensionalized dissipations. (a) SUPG dissipation on the left and (b) dynamic model/SGS dissipation on the right. Here results are with and without SUPG correction in the dynamic model with filter S1. (—): $c_1 = 16$ and SUPG correction; (---): $c_1 = 64$ and SUPG correction. (– · –): $c_1 = 16$ and no SUPG correction; (●): $c_1 = 64$ and no SUPG correction.

is large, SUPG dissipation does not have a strong impact on results and the modification to the model becomes almost negligible. It was seen that in all cases, the correction made the simulations less sensitive to even large changes to the size of the stabilization parameters.

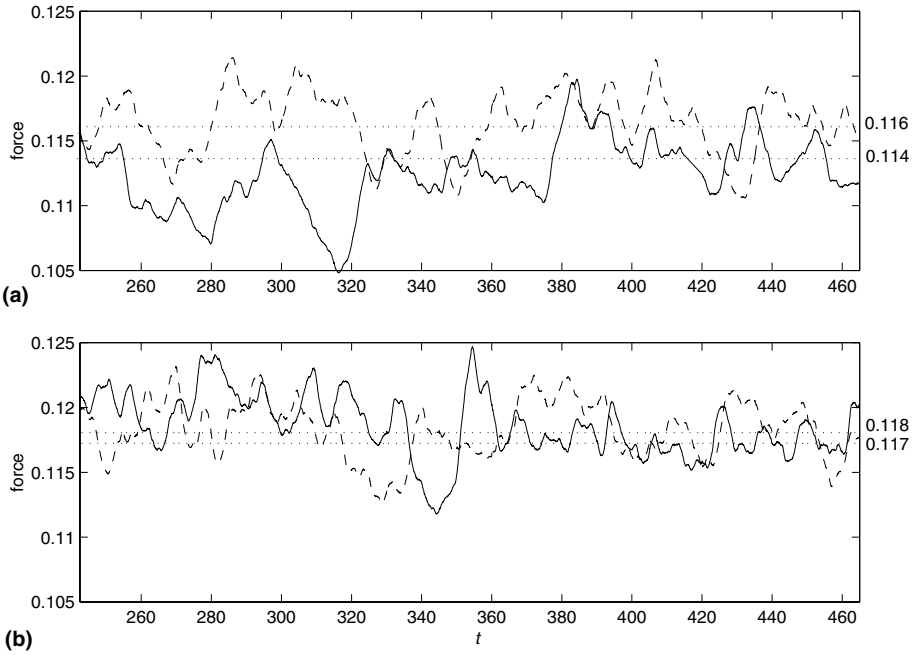

Fig. 20. (a) Wall forces without SUPG correction on the top and (b) wall forces with SUPG correction on the bottom. In all cases the model was computed with filter S1. The expected mean wall force is approximately 0.133. (—): $c_1 = 16$; (---): $c_1 = 64$.

Acknowledgments

This material is based upon work supported by the National Science Foundation under Grant No. 9985340. This work was also partially supported by the National Computational Science Alliance under Grant No. MCA01S014 and utilized the Origin2000 Array. We acknowledge Farzin Shakib of Acusim Software for the use of their linear equation solving libraries.

References

[1] C. Baiocchi, F. Brezzi, L.P. Franca, Virtual bubbles and the Galerkin/least squares method, Comput. Methods Appl. Mech. Engrg. 105 (1993) 125–142.
[2] J.P. Boris, F.F. Grinstein, E.S. Oran, R.L. Kolbe, New insights into large eddy simulation, Fluid Dyn. Res. 10 (1992) 199–228.
[3] A.N. Brooks, T.J.R. Hughes, Streamline upwind/Petrov–Galerkin formulations for convection dominated flows with particular emphasis on the incompressible Navier–Stokes equations, Comput. Methods Appl. Mech. Engrg. 32 (1982) 199–259.
[4] R. Codina, J. Blasco, Analysis of a stabilized finite element approximation of the transient convection–diffusion-reaction equation using orthogonal aubscales, Comput. Visualization Sci. 4 (2002) 167–174.
[5] M. Germano, U. Piomelli, P. Moin, W.H. Cabot, A dynamic subgrid-scale eddy viscosity model, Phys. Fluids 3 (1991) 1760.
[6] G. Hauke, T.J.R. Hughes, A comparative study of different sets of variables for solving compressible and incompressible flows, Comput. Methods Appl. Mech. Engrg. 153 (1998) 1–44.
[7] K. Horiuti, The role of the Bardina model in large eddy simulation of turbulent channel flow, Phys. Fluids A (1989) 426–428.
[8] T.J.R. Hughes, Multiscale phenomena: Green's functions, the Dirichlet-to-Neumann formulation, subgrid scale models, bubbles and the origins of stabilized methods, Comput. Methods Appl. Mech. Engrg. 127 (1995) 387–401.
[9] T.J.R. Hughes, L.P. Franca, M. Balestra, A new finite element formulation for fluid dynamics: V. A stable Petrov–Galerkin formulation of the Stokes problem accommodating equal-order interpolations, Comput. Methods Appl. Mech. Engrg. 59 (1986) 85–99.

[10] T.J.R. Hughes, L. Mazzei, K.E. Jansen, Large-eddy simulation and the variational multiscale method, Comput. Visualization Sci. 3 (2000) 47–59.
[11] T.J.R. Hughes, The Finite Element Method: Linear Static and Dynamic Finite Element Analysis, Prentice Hall, Englewood Cliffs, NJ, 1987.
[12] K.E. Jansen, C.H. Whiting, G.M. Hulbert. A generalized-α method for integrating the filtered Navier–Stokes equations with a stabilized finite element method. Comput. Methods Appl. Mech. Engrg., 1999. Contributed to a special volume devoted to the Japan–US Symposium on F.E.M. in Large-Scale C.F.D., SCOREC Report 10-1999.
[13] J. Kim, P. Moin, R. Moser, Turbulence statistics in fully developed channel flow at low Reynolds number, J. Fluid Mech. 177 (1987) 133.
[14] D. Knight, G. Zhou, N. Okong'o, V. Shukla, Compressible large eddy simulation using unstructured grids. Number 98-0535. AIAA Annual Meeting and Exhibit, 1998.
[15] D.K. Lilly, A proposed modification of the Germano subgrid–scale closure, Phys. Fluids 3 (1992) 2746–2757.
[16] T.S. Lund, On the use of discrete filters for large-eddy simulatio, in: Annual Research Briefs, NASA Ames/Stanford University, 1997. Center for Turbulence Research, pp. 83–95.
[17] R.D. Moser, J. Kim, N.N. Mansour, Direct numerical simulation of turbulent channel flow up to $Re_\tau = 590$, Phys. Fluids 11 (1999) 943–945.
[18] F.M. Najjar, D.K. Tafti, Study of discrete test filters and finite difference approximations for the dynamic subgrid-stress model, Phys. Fluids 8 (1996) 1076–1088.
[19] Okong'o, D. Knight. Compressible large eddy simulation using unstructured grids: channel and boundary layer flows. Number 98-3315. AIAA Annual Meeting and Exhibit, 1998.
[20] S.B. Pope, Turbulent Flows, Cambridge University Press, 2000.
[21] W.C. Reynolds, The potential and limitations of direct and large eddy simulations, in: J.L. Lumley (ed.), Whither Turbulence? Turbulence at the Crossroads, volume 357 of Lecture Notes in Physics. Berlin: Springer-Verlag, 1990, pp. 313–343.
[22] F. Shakib, Finite element analysis of the compressible Euler and Navier–Stokes equations. PhD thesis, Stanford University, 1989.
[23] J. Smagorinsky, General circulation experiments with the primitive equations, I. The basic experiment, Monthly Weather Rev. 91 (1963) 99–152.
[24] T. Tamura, K. Kuwahara, Numerical analysis on aerodynamic characteristics of an inclined square cylinder. Number 89-1805. AIAA Annual Meeting and Exhibit, 1989.
[25] C.A. Taylor, T.J.R. Hughes, C.K. Zarins, Finite element modeling of blood flow in arteries, Comput. Methods Appl. Mech. Engrg. 158 (1998) 155–196.
[26] A.E. Tejada-Martínez, Dynamic subgrid-scale modeling for large-eddy simulation of turbulent flows with a stabilized finite element method. PhD thesis, Rensselaer Polytechnic Institute, Nov. 2002.
[27] A.E. Tejada-Martínez, K.E. Jansen, Spatial test filters for dynamic model large-eddy simulation on finite elements, Commun. Numer. Methods Engrg. 19 (2003) 205–213.
[28] C.H. Whiting, K.E. Jansen, A stabilized finite element method for the incompressible Navier–Stokes equations using a hierarchical basis, Int. J. Numer. Methods Fluids 35 (2001) 93–116.
[29] Y. Zang, R.L. Street, J.R. Koseff, A dynamic mixed subgrid-scale model and its application to turbulent recirculating flows, Phys. Fluids A 5 (1993) 3186.